Structure and Properties of Nanocomposites Based on Poly(butylene succinate) and Organically Modified Montmorillonite

Suprakas Sinha Ray,[1] Kazuaki Okamoto,[2] Masami Okamoto[1]

[1]*Advanced Polymeric Nanocomposite Materials Laboratory, Toyota Technological Institute, Hisakata 2-12-1, Tempaku, Nagoya 468 8511, Japan*
[2]*Nagoya Municipal Research Institute, Rokuban 3-4-41, Atsuta, Nagoya 456-0058, Japan*

Received 9 June 2005; accepted 13 November 2005
DOI 10.1002/app.23940
Published online in Wiley InterScience (www.interscience.wiley.com).

ABSTRACT: Poly(butylene succinate) and organically modified montmorillonite nanocomposites with there different compositions were prepared via melt blending in a twin-screw extruder. The structure of the nanocomposites was studied with X-ray diffraction and transmission electron microscopy, which revealed the formation of intercalated nanocomposites, regardless of the silicate loading. Dynamic mechanical analysis revealed a substantial increase in the storage modulus of the nanocomposites over the entire temperature range investigated. The tensile property measurements showed a relative increase in the stiffness with a simultaneous decrease in the yield strength in comparison with that of neat poly(butylene succinate). The oxygen gas barrier property of neat poly(butylene succinate) improved after nanocomposite preparation with organically modified montmorillonite. The effect of the layered-silicate loading on the melt-state linear viscoelastic behavior of the intercalated nanocomposites was also investigated. © 2006 Wiley Periodicals, Inc. J Appl Polym Sci 102: 777–785, 2006

Key words: biodegradable polymer; organoclay; nanocomposites

INTRODUCTION

In recent years, a broad range of synthetic biodegradable resins based on synthetic aliphatic polyesters and their copolymers have been commercialized by various companies. The demand for biodegradable materials with suitable properties is said to be growing at a rapid rate. Synthetic polyesters are generally made by a polycondensation method, and raw materials are obtained from petrochemical feed stocks. Unlike other petrochemical-based resins that take centuries to degrade after disposal, these polymers break down rapidly into carbon dioxide, water, and humus under appropriate conditions when they are exposed to the combined attack of water and microorganisms. These products meet advanced composting standards and typically break down in 12 weeks under aerobic conditions.[1]

One of the most promising synthetic aliphatic polyesters in this direction is poly(butylene succinate) (PBS). It is chemically synthesized by the polycondensation of 1,4-butanediol with succinic acid. PBS has many interesting properties: biodegradability, melt processability, and thermal and chemical resistance. It has excellent processability, so it can be processed in the field of textiles into melt-blown, multifilament, monofilament, flat, and split yarn and also in the field of plastics into injection-molded products, thus being a promising polymer for various applications.[2]

Increasing our understanding of the various intrinsic properties of PBS, coupled with the knowledge of how such properties can be improved to achieve suitability for the thermoplastic processing, manufacturing, and end-use requirements, has fuelled technological and commercial interest in PBS.

Of particular interest are recently developed nanocomposites consisting of a polymer and organically modified layered silicate (OMLS), which often exhibit remarkably improved properties in comparison with those of the virgin polymer.[3–6] In general, it is believed that these concurrent property improvements in nanocomposites come from interfacial interactions between the polymer matrix and OMLS as opposed to the conventional composites.[7] The layered silicates have a layer thickness on the order of ~ 1 nm and a very high aspect ratio (10–1000). A little layered silicate (a few weight percent), well dispersed throughout the polymer matrix, thus creates much more surface area for polymer/filler interaction than conventional composites do.

Correspondence to: S. Sinha Ray, Department of Chemical Engineering, Laval University, Sainte-Foy, Quebec G1K 7P4, Canada (suprakas.sinha-ray.1@ulaval.ca); M. Okamoto (okamoto@toyota-ti.ac.jp).

In a natural extension of our ongoing research on the preparation, characterization, and properties of biodegradable polylactide/OMLS nanocomposites,[8–11] we have applied this nanocomposite technology to PBS to obtain materials with improved properties suitable for a wide range of applications.

The main objective of this article is to report the preparation, characterization, and mechanical properties of PBS/octadecyltrimethylammonium-modified montmorillonite (qC18MMT) nanocomposites in detail. The rheology of neat PBS and its corresponding nanocomposites in a molten state is also described.

EXPERIMENTAL

Materials

PBS [glass-transition temperature (T_g) = −30°C and melting temperature = 115°C] in this study was a commercial product of Showa Denko (Tokyo, Japan) with the designation Bionolle 1020. The high-molecular-weight PBS used in this study was prepared by a coupling reaction of relatively low-molecular-weight PBS (weight-average molecular weight = 50,000 g/mol) in the presence of hexamethylene diisocyanate (OCN–C_6H_{12}–NCO) as a chain extender.[12] PBS was dried in an airflow oven at 50°C for 36 h before use.

The organically modified montmorillonite (MMT) used in this study (qC18MMT) was supplied by Hojun Yoko Co. (Tokyo, Japan). According to the supplier, the original clay was MMT (cation-exchange capacity = 90 meqiv/100 g, original thickness ~ 1 nm, and length ~ 100–130 nm), which was modified with the octadecyltrimethylammonium cation.

Preparation of the nanocomposites

The nanocomposites were prepared with a twin-screw extruder (KZW15-30TGN, Technovel Corp., Tokyo, Japan) operated at 150°C. The PBS/qC18MMT master batch was first prepared by the addition of the qC18MMT powder from the window of the extruder barrel to the PBS melts. The prepared master batch and PBS pellets were dry-mixed via shaking in a bag. The mixture was then melt-extruded with the same twin-screw extruder operated at 150°C to yield nanocomposite strands. Henceforth, the product nanocomposite is abbreviated PBSCN. PBSCNs prepared with three different concentrations of MMT (inorganic part)—2.0, 3.6, and 5.4 wt %—were correspondingly abbreviated PBSCN2.0, PBSCN3.6, and PBSCN5.4. The strands were pelletized and dried *in vacuo* at 75°C for 7 h before the samples for various characterizations were molded.

The molded samples were then annealed at 60°C for 1.5 h to crystallize isothermally before being subjected to various characterizations (except for the melt rheology measurements). The contents of the inorganic parts in each nanocomposite were measured by the burning of the sample pellets at 950°C in a furnace.

Characterization methods and property measurements

Gel permeation chromatography (GPC)

The molecular weights of the PBS matrix (before and after nanocomposite preparation) were determined by GPC, with a Jasco LC-2000 Plus system (Jasco International Co., Ltd., Tokyo, Japan) and a Shodex K-804L column, with polystyrene standards for calibration and chloroform as a carrier solvent at 40°C at a flow rate of 1 mL/min. In the case of nanocomposite samples, the inorganic silicate particles were removed by means of filtration with a special type of filter before being subjected to GPC measurements.

X-ray diffraction (XRD)

The XRD patterns of pure qC18MMT powder and PBSCNs were recorded on a Maxlabo X-ray diffractometer (Tokyo, Japan). The beam was Cu Kα radiation (λ = 0.154 nm) operated at 40 kV and 20 mA. Data were obtained from 2θ = 1–10° at a scanning speed of 0.12°/min. The basal spacing of the qC18MMT before and after intercalation was estimated from the position of the d_{001} peak in the XRD pattern.

Transmission electron microscopy (TEM)

The dispersibility of the intercalated MMT layers in the PBS matrix was examined by TEM (H-7100 instrument, Hitachi, Tokyo, Japan) at an accelerating voltage of 100 kV. The TEM specimens were approximately 100 nm thick. They were prepared by the ultramicrotoming of the PBSCNs with a diamond knife.

Dynamic mechanical analysis (DMA)

The dynamic mechanical properties of neat PBS and various PBSCNs were measured with a Rheometrics RDAII (Rheometrics Scientific, Piscataway, NJ, USA) dynamic analyzer in the tension–torsion mode. The temperature dependence of the dynamic storage modulus (G'), loss modulus (G''), and their ratio (tan δ) was measured at a constant frequency (ω) of 6.28 rad/s, at a strain amplitude of 0.05%, and in the temperature range of −50 to 110°C at a heating rate of 2°C/min. The linear viscoelastic zone was assessed by the performance of strain sweep tests at ω = 6.28 rad/s. The size of the test samples was 12 × 29 × 0.7 mm^3.

TABLE I
GPC Results for Neat PBS and Corresponding Nanocomposites

Samples	$M_w \times 10^{-3}$ (g/mol)[a]	M_w/M_n[b]
PBS	101	2.4
PBSCN2.0	107	2.4
PBSCN3.6	112	2.4
PBSCN5.4	109	2.4

[a] Weight-average molecular weight.
[b] Weight-average molecular weight/number-average molecular weight.

Tensile properties

Dried PBS and various PBSCN pellets were injection-molded with a minimixer as an injector (CS-183MMX, CSI) operated at 150°C without control of the mold temperature. The tensile properties of the injection-molded samples (crystallized at 60°C for 1.5 h) were measured with an Instron 4505 instrument at room temperature. The distance of the chuck was 20 mm, and the crosshead speed was 5 mm/min.

Oxygen (O_2) gas permeability

The O_2 gas transmission rates of neat PBS and various PBSCNs were measured at 20°C and 90% relative humidity by the ASTM D 1434 differential pressure method (GTR-30XAU, Yanaco Co., Kyoto, Japan). The test samples were prepared by compression molding (thickness $\sim$ 300 μm).

Melt rheology

Melt rheology measurements were conducted on the RDAII instrument with a torque transducer capable of measurements over the range of 0.2–200 g cm. Dynamic oscillatory-shear measurements were performed by the application of a time-dependent strain of $\gamma(t) = \gamma_0 \sin(\omega t)$ (where γ_0 is the initial strain and t is the time), and the resultant shear stress was $\sigma(t) = \gamma_0[G' \sin(\omega t) + G'' \cos(\omega t)]$. The measurements were conducted with a set of 25-mm-diameter parallel plates with a sample thickness of $\sim$1.5 mm and in the temperature range of 120–150°C. The strain amplitude was fixed at 5% to obtain reasonable signal intensities even at elevated temperatures or at low ω values to avoid the nonlinear response. For each nanocomposite investigated, the limits of the linear viscoelasticity were determined by the performance of strain sweeps at a series of fixed ω values. The master curves were generated with the principle of time–temperature superposition and shifted to a common reference temperature (T_{ref}) of 120°C, which was chosen as the most representative of a typical processing temperature of PBS.

Steady-shear viscosity measurements were conducted at 120°C with 25-mm-diameter cone-and-plate geometry with a cone angle of 0.1 rad. The steady-shear viscosity data reported in this article were obtained as a function of the shear rate and time at different shear rates.

RESULTS AND DISCUSSION

GPC

The results of the GPC measurements are summarized in Table I. The GPC data clearly indicate that there is almost no degradation of the PBS matrix after nanocomposite preparation with qC18MMT.

Nanocomposite structure

The nanocomposite structure has typically been elucidated with XRD patterns and TEM observations. XRD patterns offer a convenient method for determining the interlayer spacing of the silicate layers in the pure organoclay and in the intercalated polymer/clay nanocomposites. On the other hand, TEM observations allow a qualitative understanding of the internal structure through direct visualization. XRD patterns for the pure qC18MMT powder and representative PBSCNs are presented in Figure 1. The mean interlayer spacing of the (001) plane [$d_{(001)}$] for the qC18MMT powder obtained by XRD measurements is 1.93 nm ($2\theta \cong 4.56°$). In the case of PBSCN2.0, a small peak can be observed at $2\theta = 2.97°$, corresponding to the (001) plane of the dispersed silicate layers in the PBS matrix. With increasing MMT content, this peak becomes stronger and gradually shifts toward the higher diffraction angle at $2\theta = 3.11°$ ($\cong$2.84 nm) for PBSCN5.4. The difference in the interlayer spacing between the pure qC18MMT powder and PBSCN2.0 to PBSCN5.4 after melt mixing is presumably due to the intercalation of PBS chains into the silicate galleries, and the coherent order of the silicate layers also systematically increases with increasing MMT content. The existence of a sharp Bragg peak in the PBSCNs after melt extrusion clearly indicates that the dispersed silicate layers retain an ordered structure after melt extrusion.

The width of the XRD peak (β; measured by the full width at half-maximum) is inversely proportional to the coherence length of the scattering intensity (D) and therefore reflects the coherent order of the silicate layers:[13]

$$D = (\lambda k)/(\beta \cos \theta)$$

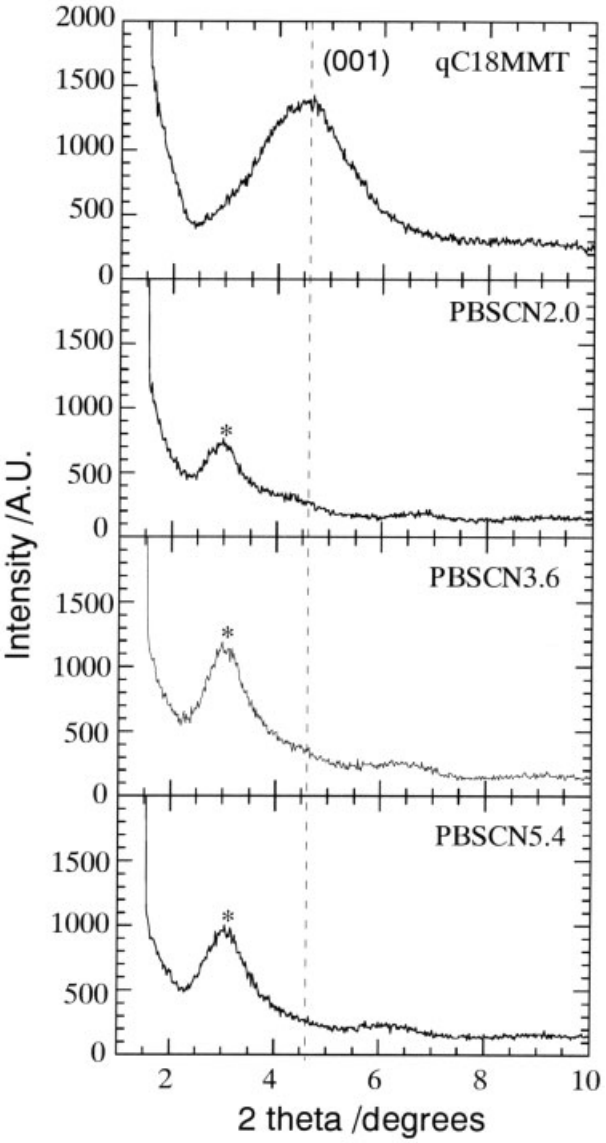

Figure 1 XRD patterns of pure qC18MMT powder and corresponding nanocomposites of PBS. The dashed line indicates the location of the silicate (001) reflection of qC18MMT, and the asterisks indicate the (001) peak of qC18MMT dispersed in the PBS matrix.

where k is a constant and generally equal to 0.9, λ is 0.154 nm, and θ is the wide-angle XRD peak position. This equation is known as the Scherrer equation, and it is not fully applicable to intercalated nanocomposite systems because these are not ideal crystallized lamellae. However, we can get approximate data about the stacking of the individual silicate layers by applying the Scherrer equation.

Because the width and intensity of the basal spacing of qC18MMT decrease sharply after nanocomposite preparation with PBS, the coherence of the intercalated silicate layers is much higher than that of the unintercalated silicate layers. Thus, XRD analyses indicate that PBS melt extrusion has a strong effect on the layer structure of qC18MMT and significantly changes the coherence length of the silicate crystallites.

The internal structure of the nanocomposites on a nanometer scale has been directly observed via TEM images. Figure 2(a–d) shows bright-field TEM images of two different PBSCNs corresponding to the XRD patterns shown in Figure 1; the dark entities are the cross sections of intercalated qC18MMT layers [because the silicate layers are composed of heavier elements (Al, Si, and O) than the interlayer and surrounding matrix (C, H, N, etc.), they appear darker in bright-field images].[14] The figure shows both a larger view, showing the dispersion of the MMT within the PBS matrix, and a higher magnification, permitting the observation of discrete silicate layers. TEM images of PBSCN2.0 [Fig. 2(a,b)] indicate that the silicate layers are intercalated, stacked, and homogeneously distributed in the PBS matrix. On the other hand, in the case of PBSCN5.4 with a higher MMT content [Fig. 2(c,d)], random orientation of the silicate layers to the matrix surface can be observed.

The form factors obtained from XRD patterns and TEM observations, that is, the average length (L_{LS}) and thickness (d_{LS}) of the dispersed intercalated MMT layers and the correlation length (ξ_{LS}) between them, are summarized in Table II. Thus, XRD analyses and TEM observations clearly indicate that PBSCNs prepared with

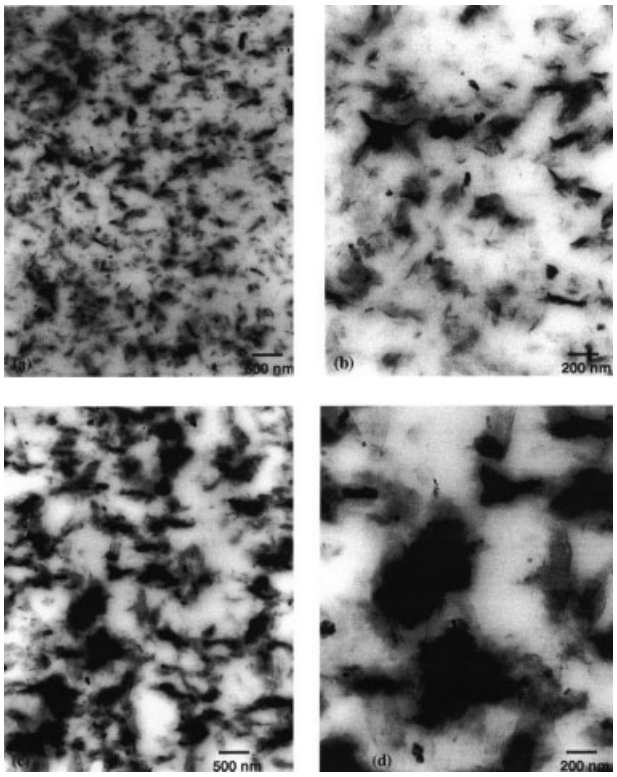

Figure 2 Bright-field TEM images of PBSCNs: (a) PBSCN2.0 (40,000×), (b) PBSCN2.0 (100,000×), (c) PBSCN5.4 (40,000×), and (d) PBSCN5.4 (100,000×). The dark entities are the cross sections of the intercalated silicate layers.

qC18MMT lead to the formation of well-ordered intercalated nanocomposites with stacked and flocculated structures, and the coherence order of the silicate layers gradually increases with increasing MMT content.

Nanocomposite properties

DMA

DMA was used to track the temperature dependence of G', G'', and tan δ of neat PBS upon nanocomposite formation with qC18MMT. Figure 3 shows the temperature dependence of G', G'', and tan δ of neat PBS and various PBSCNs. For all PBSCNs, a significant enhancement of G' has been observed in the investigated temperature range in comparison with that of the neat matrix, indicating that qC18MMT has a strong effect on the elastic properties of neat PBS. Below T_g, there is also a strong enhancement of G' for all PBSCNs.

On the other hand, above T_g, the enhancement of G'' is significant in the intercalated PBSCNs in comparison with that below T_g, indicating that a plastic response to the deformation is prominent in the presence of qC18MMT when the material becomes soft. However, the presence of qC18MMT particles does not lead to a significant shift and broadening of the tan δ curves for the PBSCNs in comparison with that of neat PBS. This behavior can be ascribed to the unrestricted segmental motions at the organic–inorganic interface neighborhood of intercalated PBSCNs.

Tensile properties

Figure 4 presents the tensile properties of neat PBS and various PBSCNs measured at 25°C. There is a slight increase in the tensile modulus for PBSCN2.0 in comparison with that of neat PBS, followed by a significant increase with increasing MMT content and a maximum of 69% for PBSCN5.4. On the other hand, the tensile strength gradually decreases with increasing MMT content.

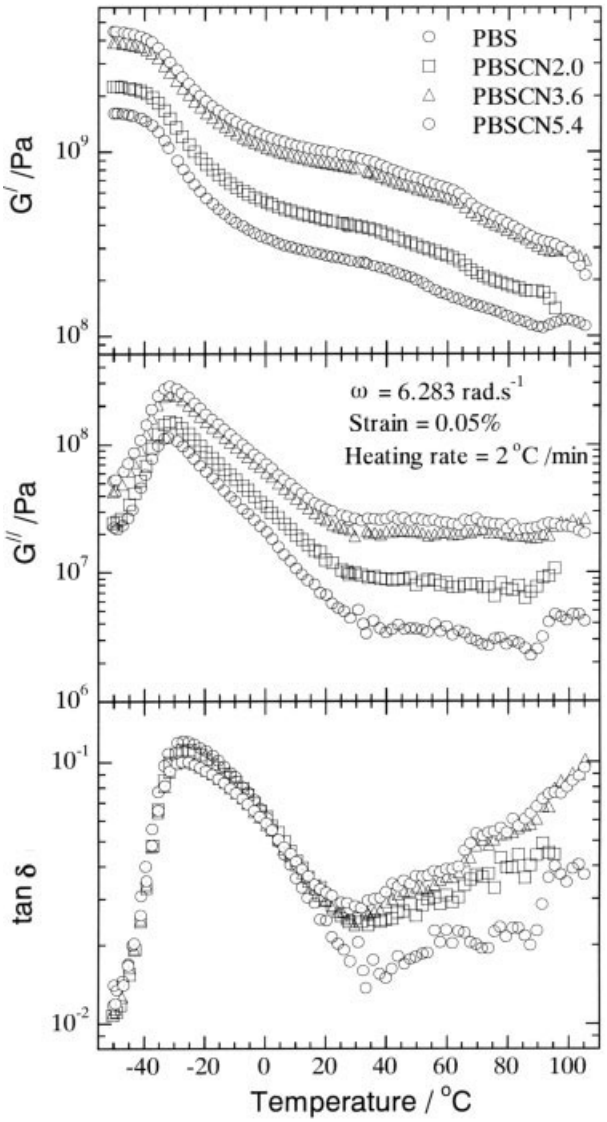

Figure 3 Temperature dependence of G', G'', and tan δ of neat PBS and three different PBSCNs.

TABLE II
Form Factors of Nanocomposites Obtained from XRD Patterns and TEM Observations

	PBSCN2.0	PBSCN3.6	PBSCN5.4
XRD			
$d_{(001)}$ (nm)	2.97	2.87	2.84
$\Delta d_{(001)}$ (nm)[a]	1.04	0.94	0.91
d_{LS} (nm)[b]	11.35	11.51	11.53
TEM			
L_{LS} (nm)	355 ± 21	738 ± 60	781 ± 14
ξ_{LS} (nm)	81 ± 13	72 ± 27	68 ± 11
L_{LS}/d_{MMT}	~31.3	~64.1	~67.7

[a] Extent of intercalation: $\Delta d_{(001)} = d_{PBSCN} - d_{OMLS}$.
[b] $d_{LS} \cong D$ (calculated on the basis of the Scherrer equation).[13] d_{PBSCN} is the $d_{(001)}$ spacing for nanocomposites. d_{OMLS} is the $d_{(001)}$ spacing for OMLS.

O_2 gas permeability

The layered silicates are believed to increase the gas barrier properties of nanocomposites by creating a maze or tortuous path that retards the progress of gas molecules through the matrix resin.[3,15] Figure 5 presents the O_2 gas permeability for the neat PBS and various PBSCN sheets. The barrier property of PBS is not significantly improved after nanocomposite preparation with qC18MMT. This may be due to the high degree of crystallinity in the case of nanocomposites in the presence of MMT in comparison with that of neat PBS because in nanocomposites the clay particles act as nucleators for crystallization.[16]

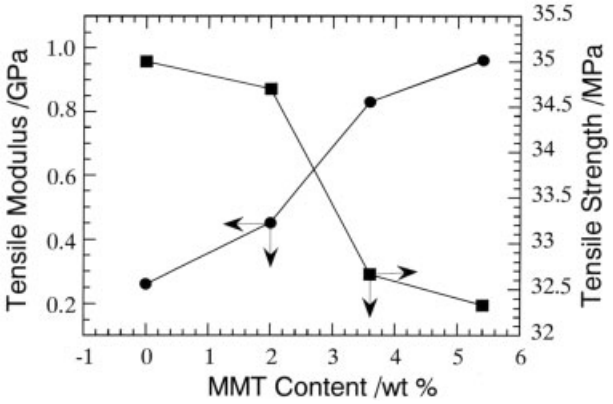

Figure 4 Tensile properties of neat PBS and various PBSCNs.

Melt rheology

The measurement of the melt rheology properties of polymer/layered-silicate nanocomposites is crucial to gain a fundamental understanding of the processability and structure–property relationship of these materials. Generally, the rheology of polymer melts depends strongly on the temperature at which the measurement is carried out. In the case of our polymer samples, it was expected that, at the temperatures and ω values at which the rheological measurements were carried out, characteristic homopolymer-like terminal flow behavior would be exhibited [expressed by the power laws $G'(\omega) \propto \omega^2$ and $G''(\omega) \propto \omega$].

The master curves for $G'(\omega)$ and $G''(\omega)$ of neat PBS and various PBSCNs with silicate loadings of different weight percentages are presented in Figure 6. At high ω values ($a_T\omega > 5$, where a_T is the temperature-dependent frequency shift factor), the viscoelastic behavior of all the PBSCNs is the same, with the exception of only a systematic increase in the modulus value with increasing silicate content. On the other hand, at low ω values ($a_T\omega < 5$), both moduli exhibit a weak ω dependence with increasing MMT content, and this means that there are gradual changes in the behavior from liquidlike [$G'(\omega) \propto \omega^2$ and $G''(\omega) \propto \omega$)] to solidlike with increasing MMT content.

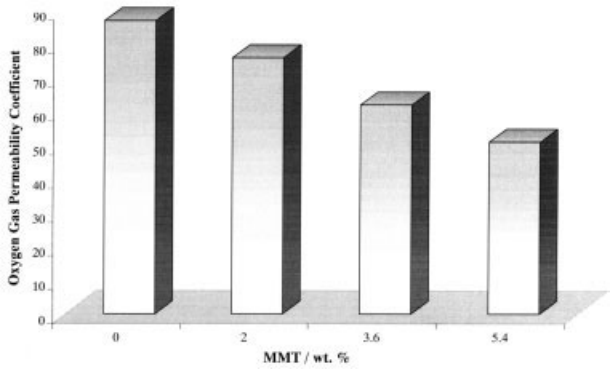

Figure 5 Oxygen gas permeability coefficient of various PBSCNs as a function of the MMT content.

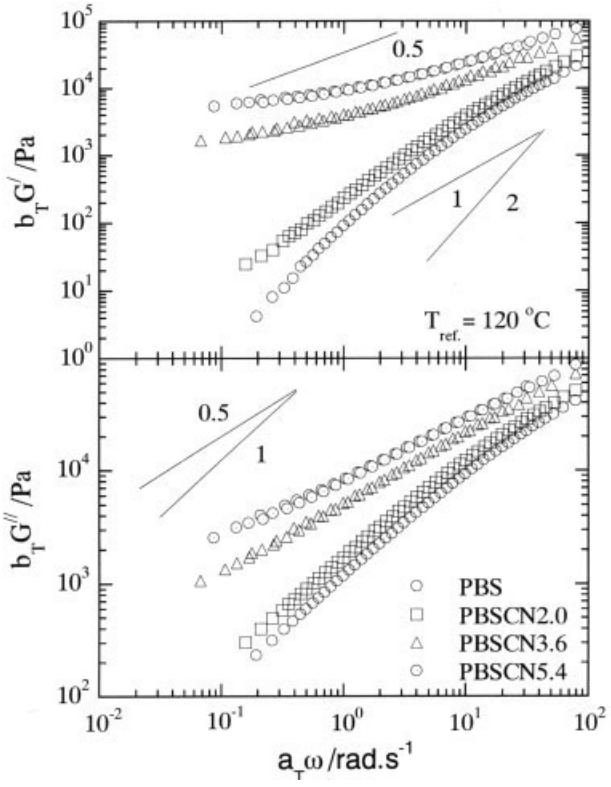

Figure 6 Reduced ω dependence of $G'(\omega)$ and $G''(\omega)$ of neat PBS and various PBSCNs. b_T is the horizontal shift factor.

The terminal-region slopes of the master curves for $G'(\omega)$ and $G''(\omega)$ are presented in Table III. The slopes of $G'(\omega)$ and $G''(\omega)$ in the terminal region of the master curves of the PBS matrix are 1.8 and 1, respectively, and these values are in the range expected for polydisperse polymers.[17] On the other hand, the slopes of $G'(\omega)$ and $G''(\omega)$ are considerably lower for all PBSCNs in comparison with those of neat PBS with a similar molecular weight and polydispersity. In fact, for PBSCNs with high MMT contents, $G'(\omega)$ becomes nearly independent at low $a_T\omega$ values and exceeds $G''(\omega)$; this is characteristic of materials exhibiting a pseudo-solidlike behavior.

TABLE III
Terminal-Region Slopes of $G'(\omega)$ and $G''(\omega)$ Versus $a_T\omega$ (<10 rad/s) for Neat PBS and PBSCNs

	Slope	
Sample	$G'(\omega)$	$G''(\omega)$
PBS	1.8	1
PBSCN2.0	1.2	0.8
PBSCN3.6	0.3	0.4
PBSCN5.4	0.2	0.26

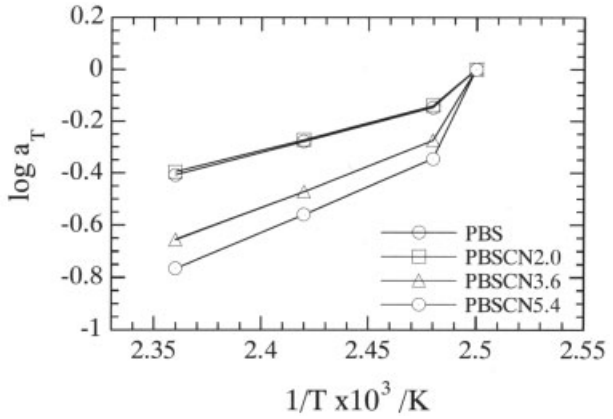

Figure 7 a_T of neat PBS and various PBSCNs as a function of temperature (T).

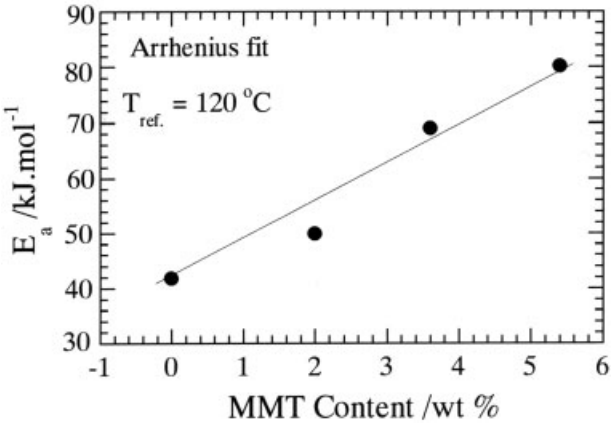

Figure 8 E_a as a function of the MMT content.

Table II shows that the ξ_{LS} values of PBSCNs are smaller than L_{LS}, suggesting the formation of a spatially linked structure of the dispersed MMT particles in the PBS matrix.[17] According to this structure, the individual stacked silicate layers are incapable of freely rotating (only translational motion is available), and hence the relaxation of the structure by the imposition of a small ω value is prevented almost completely with a high MMT content.[17] This type of prevented relaxation due to highly geometric constraints or physical jamming of the stacked silicate layers leads to the presence of pseudo-solid-like behavior, as observed for PBSCN3.6 and PBSCN5.4. The formation of this type of spatially linked structure in PBSCNs with high MMT contents in the molten state is also confirmed by the lower slope values and the higher absolute values of the dynamic moduli in the case of PBSCNs.[18]

a_T, used to generate master curves, is shown in Figure 7. The dependence of a_T on the MMT loading suggests that the temperature-dependent relaxation processes of the PBS melt observed in the viscoelastic measurements are affected by the presence of silicate layers, and the deviation is significant with high MMT contents. This behavior is different from that so far reported in a study on polymer/OMLS nanocomposites, which showed the complete independence of a_T of the OMLS loading, indicating that the temperature-dependent relaxations observed in the case of neat polymers under viscoelastic measurements are unaffected in the presence of silicate layers.[19,20] This behavior may be due to the strong interaction between the PBS matrix and OMLS by the formation of hydrogen bonds, as discussed previously.[17]

Figure 8 presents the MMT content dependence (wt %) of the flow activation energy (E_a) of neat PBS and various PBSCNs obtained from an Arrhenius fit of the master curves. E_a systematically increases with increasing MMT content in the case of PBSCNs. This observation indicates that with high MMT contents, it is very difficult for the materials to flow. This behavior is also ascribed to the formation of a spatially linked structure in PBSCNs with high MMT contents in the molten state.

The dynamic complex viscosity [$|\eta^*|(\omega)$] master curves for the neat PBS and various PBSCNs, based on linear dynamic oscillatory-shear measurements, are presented in Figure 9. In a low $a_T\omega$ region (<10 rad/s), neat PBS exhibits almost Newtonian behavior, whereas all PBSCNs show a very strong shear-thinning tendency. On the other hand, the weight-average molecular weights and polydispersity indices of neat PBS and PBSCNs are almost the same, so the high viscosity of PBSCNs can be explained by the flow restrictions of polymer chains in the molten state due to the presence of MMT particles.

The time-dependent viscosity of neat PBS and a series of intercalated PBSCNs is shown in Figure 10. The shear viscosity of PBSCNs is enhanced considerably at all shear rates with time, and at a fixed shear rate, it increases monotonically with increasing MMT

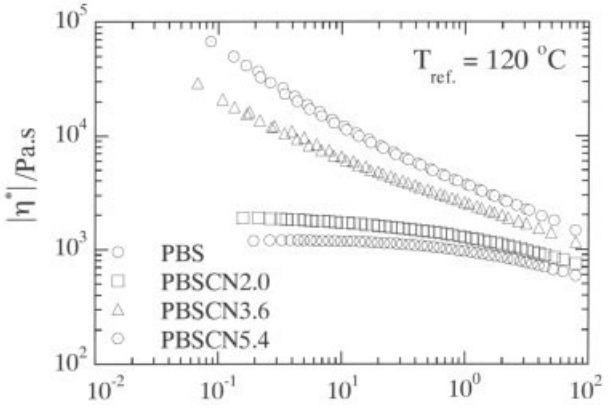

Figure 9 Reduced ω dependence of $|\eta^*|(\omega)$ of neat PBS and various PBSCNs.

loading. On the other hand, all intercalated PBSCNs exhibit strong rheopexy behavior, and this behavior becomes prominent at a low shear rate (0.001 s^{-1}), whereas neat PBS exhibits a time-independent viscosity at all shear rates. With increasing shear rates, the shear viscosity attains a plateau after a certain time, and the time required to attain this plateau decreases with increasing shear rates. A possible reason for this kind of behavior may be the planar alignment of the clay platelets toward the flow direction under shear.

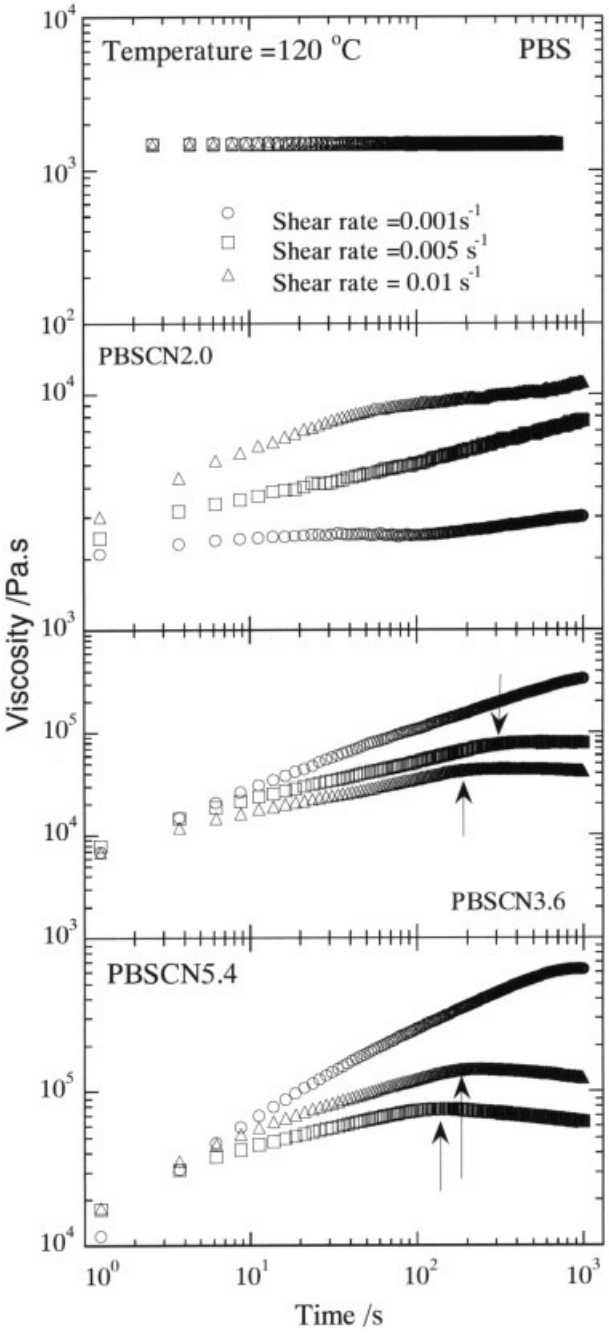

Figure 10 η of neat PBS and various PBSCNs as a function of time.

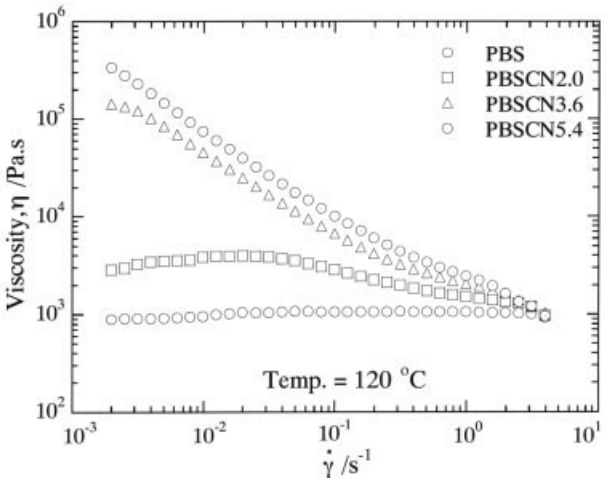

Figure 11 η of neat PBS and various PBSCNs as a function of $\dot{\gamma}$ (s^{-1}).

When the shear rate is very slow (0.001 s^{-1}), MMT particles take longer time to attain complete planar alignment along the flow direction, and this measurement time (1000 s) is too short to attain such an alignment. For this reason, PBSCNs show strong rheopexy behavior. On the other hand, under slightly higher shear rates (0.005 or 0.01 s^{-1}), this measurement time is enough to attain such an alignment, and so PBSCNs show time-independent shear viscosity after a certain time.

Figure 11 shows the shear-rate dependence of the viscosity of neat PBS and various PBSCNs measured at 120°C. Although the neat PBS exhibits almost Newtonian behavior at all shear rates, the PBSCNs exhibit non-Newtonian behavior. All PBSCNs show a very strong shear-thinning tendency at all measured shear rates, and this is analogous to the results obtained in the case of oscillatory-shear measurements (Fig. 9). Additionally, at very high shear rates, the steady-shear viscosities of PBSCNs are comparable to that of neat PBS. These observations suggest that the silicate layers are strongly aligned toward the flow direction, and shear-thinning behavior at high shear rates is dominated by that of the neat polymer.[17]

Like the other polymer/OMLS systems,[19,20] the data for the PBSCNs also exhibit a significant deviation from the Cox–Merz relation,[21] whereas neat PBS nicely obeys the empirical Cox–Merz relation, which requires that for $\dot{\gamma}=\omega$ (where $\dot{\gamma}$ is the shear rate), the viscoelastic data should obey the relationship $\eta(\dot{\gamma}) = |\eta^*|(\omega)$ (where η is the viscosity). There are two possible reasons for the deviation of the Cox–Merz relation in the case of nanocomposites: first, this rule is only applicable to homogeneous systems such as homopolymer melts, but nanocomposites are heterogeneous systems. For this reason, this relation is nicely obeyed in the case of neat PBS. Second, the structure

formation is different when nanocomposites are subjected to dynamic oscillatory-shear and steady-shear measurements.

CONCLUSIONS

Polymer/layered-silicate nanocomposites with synthetic biodegradable poly(butylene succinate) and organically modified MMT were prepared by a melt-extrusion process in a twin-screw extruder. XRD patterns and TEM observations established the formation of intercalated nanocomposites. DMA exhibited a significant increase in the modulus of the nanocomposites at room temperature. The tensile properties of the nanocomposites showed a relative increase in the modulus with a simultaneous decline in the yield strength. An improvement in the oxygen gas barrier property of neat PBS was also noted in the nanocomposites. In rheological experiments in the molten state, pseudo-solid-like behavior was observed for the nanocomposites containing 3.6 or 5.4 wt % MMT. This was attributed to the network formation of the dispersed MMT particles.

References

1. Mohanty, A. K.; Drzal, L. T.; Misra, M. Polym Mater Sci Eng 2003, 88, 60.
2. (a) Ratto, J. A.; Stenhouse, P. J.; Auerbach, M.; Fitchel, J.; Farell, R. Polymer 1999, 40, 6777; (b) Fujimaki, T. Polym Degrad Stab 1998, 59, 209.
3. Sinha Ray, S.; Okamoto, M. Prog Polym Sci 2003, 28, 1539.
4. Biswas, M.; Sinha Ray, S. Adv Polym Sci 2001, 155, 167.
5. Sinha Ray, S.; Bousmina, M. Prog Mater Sci 2005, 50, 962.
6. Giannelis, E. P.; Krishnamoorti, R.; Manias, E. Adv Polym Sci 1999, 138, 107.
7. (a) Sinha Ray, S.; Bousmina, M.; Okamoto, K. Macromol Mater Eng 2005, 290, 759; (b) Chen, J. S.; Poliks, M. D.; Ober, C. K.; Zhang, Y.; Wiesner, U.; Giannelis, E. P. Polymer 2002, 43, 4895.
8. (a) Sinha Ray, S.; Maiti, P.; Okamoto, M.; Yamada, K.; Ueda, K. Macromolecules 2002, 35, 3104; (b) Sinha Ray, S.; Okamoto, K.; Yamada, K.; Okamoto, M. Nano Lett 2002, 2, 423; (c) Sinha Ray, S.; Yamada, K.; Okamoto, M.; Ogami, A.; Ueda, K. Compos Interfaces 2003, 10, 435; (d) Nam, J. Y.; Sinha Ray, S.; Okamoto, M. Macromolecules 2003, 36, 7126.
9. (a) Sinha Ray, S.; Yamada, K.; Okamoto, M.; Ueda, K. Nano Lett 2002, 2, 1093; (b) Sinha Ray, S.; Yamada, K.; Okamoto, M.; Ueda, K. Polymer 2003, 44, 857; (c) Sinha Ray, S.; Yamada, K.; Okamoto, M.; Fujimoto, Y.; Ogami, A.; Ueda, K. Polymer 2003, 44, 6633.
10. (a) Sinha Ray, S.; Yamada, K.; Ogami, A.; Okamoto, M.; Ueda, K. Macromol Rapid Commun 2002, 23, 943; (b) Sinha Ray, S.; Yamada, K.; Okamoto, M.; Ogami, A.; Ueda, K. Chem Mater 2003, 15, 1456.
11. (a) Sinha Ray, S.; Yamada, K.; Okamoto, M.; Ueda, K. Macromol Mater Eng 2003, 288, 203; (b) Fujimoto, Y.; Sinha Ray, S.; Okamoto, M.; Ogami, A.; Ueda, K. Macromol Rapid Commun 2003, 24, 457; (c) Sinha Ray, S.; Okamoto, M. Macromol Rapid Commun 2003, 24, 815; (d) Sinha Ray, S.; Yamada, K.; Okamoto, M.; Ueda, K. J Nanosci Nanotechnol 2003, 3, 503.
12. Yasuda, T.; Takiyama, E. U.S. Pat. 5,391,644 (1995).
13. Dritis, V. A.; Tchoubar, C. X-Ray Diffraction by Disordered Lamellar Structure; Springer-Verlag: New York, 1990; Chapter 90, p 20.
14. Pinnavaia, T. J. In Chemical Physics of Intercalation; Legrand, A. P.; Flandrois, S., Eds.; Plenum: New York, 1987.
15. Bharadwaj, R. K. Macromolecules 2001, 34, 9189.
16. Maiti, P.; Nam, P. H.; Okamoto, M.; Usuki, A.; Hasegawa, N. Macromolecules 2002, 35, 2042.
17. (a) Sinha Ray, S.; Okamoto, K.; Okamoto, M. Macromolecules 2003, 36, 2356; (b) Okamoto, K.; Sinha Ray, S.; Okamoto, M. J Polym Sci Part B: Polym Phys 2003, 41, 3160.
18. Hoffmann, B.; Kressler, J.; Stopplemass, G.; Friedrich, C.; Kim, G. M. Colloid Polym Sci 2000, 278, 629.
19. Krishnamoorti, R.; Koray, Y. Curr Opin Colloid Interface Sci 2001, 6, 464.
20. Sinha Ray, S.; Okamoto, M. Macromol Mater Eng 2003, 288, 936.
21. Cox, W. P.; Merz, E. H. J Polym Sci 1958, 28, 619.